



HAL
open science

Deflection, drift and advective growth in variable-density, laminar mixing layers.

L. Bretonnet, Jean-Bernard Cazalbou, Patrick Chassaing, Marianna Braza

► **To cite this version:**

L. Bretonnet, Jean-Bernard Cazalbou, Patrick Chassaing, Marianna Braza. Deflection, drift and advective growth in variable-density, laminar mixing layers.. *Physics of Fluids*, 2007, 1 (10), pp.0.10.1063/1.2772901 . hal-03610124

HAL Id: hal-03610124

<https://hal.science/hal-03610124>

Submitted on 16 Mar 2022

HAL is a multi-disciplinary open access archive for the deposit and dissemination of scientific research documents, whether they are published or not. The documents may come from teaching and research institutions in France or abroad, or from public or private research centers.

L'archive ouverte pluridisciplinaire **HAL**, est destinée au dépôt et à la diffusion de documents scientifiques de niveau recherche, publiés ou non, émanant des établissements d'enseignement et de recherche français ou étrangers, des laboratoires publics ou privés.

Deflection, drift, and advective growth in variable-density, laminar mixing layers

L. Bretonnet, J.-B. Cazalbou,^{a)} and P. Chassaing^{b)}
 ENSICA, 1 place Émile Blouin, 31056 Toulouse Cedex 5, France

M. Braza
 Institut de Mécanique des Fluides de Toulouse, UMR 5502 CNRS, 31400 Toulouse, France

(Received 20 March 2007; accepted 24 July 2007; published online 2 October 2007)

Specific features of the variable-density mixing layers without gravity effects are studied using self-similar solutions to the laminar and time-evolving variant of this flow. Density variations come from either mass or temperature mixing, accounting for, in the latter case, the effect of the Mach number. The transverse profiles of the flow quantities, as well as the time evolutions of the global characteristic scales of the mixing layer, are given for a wide range of density ratio and Mach-number values. When compared to the constant-density case, it appears that most of the specificity of these flows comes from the emergence of a nonzero transverse component of the velocity. First, it produces a deflection of the flow that can be either confined in the core of the layer or global, the whole layer being tilted at an angle from the initial flow direction. In most cases, this deflection is such that some part of the higher-density fluid is “entrained” in the direction of the lower-density fluid, leaving no possibility to define a dividing streamline. Second, it leads to a shift between the density profile and the profiles of the other flow quantities. This shift scales on the (time-increasing) mixing-layer thickness and therefore appears as a time drift. When global deflection is present, the tilting of the layer can be shown to be equivalent to a global drift of the mixing/shear layer toward the light-fluid side of the flow. Third, transport by the transverse velocity component affects the spreading of the mixing layer, giving rise to an additional effect referred to as advective growth. Examination of the density-ratio and Mach-number effects leads to surprising results: While the momentum thickness is always observed to decrease when increasing these parameters, conventional thicknesses (based on the profiles of the different variables) can show opposite behaviors depending on the form of the diffusion model for the considered variable.
 © 2007 American Institute of Physics. [DOI: 10.1063/1.2772901]

I. INTRODUCTION

Mixing of mass, momentum, or temperature is the key to performance in a wide range of technologies, including aerodynamics, combustion, thermal engineering, and chemical engineering, among others. The basic flow configuration for studying these phenomena is the mixing layer between two parallel streams, with different densities and/or temperatures, flowing with different velocities—possibly in the compressible range. Since the work of Brown and Roshko,¹ the dependency of the spreading rate of the layer (a direct measure of the mixing efficiency) to various parameters, and the mechanisms by which mixing occurs in the variable-density case, have been studied extensively. Due to the fact that turbulence is the most frequent state of motion in a number of practical applications, it is no surprise that most of the effort has been focused on the turbulent variant of this flow. Experiment, numerical simulation, and theoretical considerations all agree on the point that the spreading rates are strongly modified when compared to those obtained in the

constant-density case. The significant parameters appear to be (i) the density ratio between the two fluids (the cases of temperature or mass inhomogeneity seem to be roughly equivalent from this point of view), (ii) the velocity ratio between the two streams (in the space-evolving configuration), and (iii) the convective Mach number (the velocity difference normalized by the average speed of sound²). Semiempirical relations such as those given by Brown³ or Dimotakis⁴ are well supported by experiment and indicate significant modifications to the spreading rate when the density and velocity ratio are varied. The well-known Langley curve gathers a substantial number of experimental data that indicate an important reduction of the spreading rate when the convective Mach number is increased. Direct numerical simulations of Vreman, Sandham, and Luo⁵ and Pantano and Sarkar⁶ have been essential to understand the mechanism by which the mixing efficiency is altered in the variable-density case. They reveal the influence of compressibility effects on the turbulent motion, which in turn modifies the mean flow. Paradoxically, the laminar situation, which is an ideal framework to investigate the *direct* influence of density variation on the global characteristics of the flow, has seldom been investigated. Sanchez, Vera, and Linan⁷ have given analyti-

^{a)}Electronic mail: cazalbou@ensica.fr

^{b)}Also at INPT-ENSEEIH-Institut de Mécanique des Fluides de Toulouse, UMR 5502 CNRS, 31400 Toulouse, France.

cal solutions to several laminar mixing problems, including the case of the time-evolving mixing layer between two gases of different densities. They give limited information on the emergence of a transverse component of velocity, which, as we shall see hereafter, is specific to the variable-density situation. Self-similar solutions have also been used by several authors (see, for example, Kozusco *et al.*⁸ and Lardjane, Fedioun, and Gökalp⁹) to initiate stability analysis or numerical simulations of dissimilar gases with different temperatures and velocities in the compressible range. These have been performed with elaborate models for the variations of the fluid properties and precise combination of gases, but do not give a systematic account of the separate effects of the different sources of density variation on the global characteristics of the flow.

In this paper, we use simple models for the fluid properties to obtain self-similar solutions to the time-evolving mixing-layer problem. Density variations due to temperature differences, use of dissimilar gases, and the compressible-flow regime are investigated separately in order to analyze the specific mechanisms involved in variable-density mixing. The problem is precisely stated in Sec. II, and the self-similarity analysis is presented in Sec. III. Calculations performed in the three different configurations are presented and discussed in Sec. IV.

II. STATEMENT OF THE PROBLEM

We consider the problem of a time-evolving variable-density mixing layer, in the case in which gravity can be neglected. At some initial time ($t=0$), the half-spaces $z < 0$ and $z > 0$ contain two parallel-flowing fluids that will be referred to as fluid A and fluid B, respectively. For the sake of brevity, the higher- and lower-density fluids will be qualified as “heavy” and “light,” respectively, although these terms would only be relevant in the presence of gravity. Initially, the velocity is aligned with x and the pressure is uniform throughout the flow. The temperature, density, and velocity of fluid A will be denoted as T_A , ρ_A , and $-U_0$ ($U_0 > 0$); those of fluid B will be denoted as T_B , ρ_B , and U_0 . The uniform value of the pressure at $t=0$ will be denoted as P_∞ and related to the state variables by the ideal-gas relation

$$P_\infty = \rho_A \mathcal{R}_A T_A = \rho_B \mathcal{R}_B T_B,$$

where \mathcal{R}_A and \mathcal{R}_B are the ideal-gas constants of fluid A and fluid B, respectively.

We are interested in one-dimensional (invariant along x and y) and unsteady (starting at $t=0$) solutions to this problem. Under these assumptions, the continuity equation $d\rho/dt + \rho \nabla \cdot \mathbf{U} = 0$ can be written as

$$\frac{\partial \rho}{\partial t} = -W \frac{\partial \rho}{\partial z} - \rho \frac{\partial W}{\partial z},$$

where W denotes the transverse velocity component (along z). Setting $W=0$ in the above equation leads to the obviously incorrect result that the density will remain constant in the flow at any location and at any time. It appears, therefore, that, contrary to the constant-density case, variable-density mixing layers necessarily involve some *deflection* of the flow

(that is, nonzero values of the transverse velocity component).

The above simple argument further points out the connection between deflection and divergence of the velocity field ($\equiv \partial W / \partial z$), and prompts one to examine the possible causes for a nonzero divergence. To this end, we introduce the mass fraction C of fluid A (also called concentration below), and write the equations of the problem for a mixture of Newtonian fluids following the Fourier and Fick laws, in the absence of cross-diffusion effects such as the Dufour and Soret effects (see, for example, Chassaing *et al.*¹⁰),

$$P = \rho(a^* C + b^*)T, \quad (1)$$

$$\frac{d\rho}{dt} = -\rho \frac{\partial W}{\partial z}, \quad (2)$$

$$\rho \frac{dU}{dt} = \frac{\partial}{\partial z} \left(\mu \frac{\partial U}{\partial z} \right), \quad (3)$$

$$\rho \frac{dW}{dt} = -\frac{\partial P}{\partial z} + \frac{4}{3} \frac{\partial}{\partial z} \left(\mu \frac{\partial W}{\partial z} \right), \quad (4)$$

$$\rho \frac{dC}{dt} = \frac{\partial}{\partial z} \left(\rho D \frac{\partial C}{\partial z} \right), \quad (5)$$

$$\rho \frac{d(C_p T)}{dt} = -\frac{dP}{dt} + \frac{4}{3} \mu \left(\frac{\partial W}{\partial z} \right)^2 + \mu \left(\frac{\partial U}{\partial z} \right)^2 + \frac{\partial}{\partial z} \left(\lambda \frac{\partial T}{\partial z} \right). \quad (6)$$

In these equations, μ , λ , D , and C_p denote, respectively, the molecular viscosity, thermal conductivity, mass diffusivity, and specific heat at constant pressure. The equation of state (1) involves two constants a^* and b^* connected to the universal ideal-gas constant \mathcal{R} and molecular weights \mathcal{M}_A and \mathcal{M}_B of the two fluids through the relations

$$a^* = \mathcal{R} \frac{\mathcal{M}_B - \mathcal{M}_A}{\mathcal{M}_A \mathcal{M}_B} \quad \text{and} \quad b^* = \frac{\mathcal{R}}{\mathcal{M}_B}.$$

We may already mention that changing the sign of U leaves the system (1)–(6) unchanged. It follows that—contrary to the space-evolving mixing layer—the time-evolving mixing layer has the same behavior in the cogradient ($\partial \rho / \partial z \times \partial U / \partial z > 0$) and countergradient ($\partial \rho / \partial z \times \partial U / \partial z < 0$) situations. As a consequence, we can adopt, without any loss of generality, the convention that index B always denotes the heavier fluid. Now, following Chassaing¹¹ or Lele,¹² we can write an equation for the divergence of the velocity field ($\nabla \cdot \mathbf{U} \equiv \partial W / \partial z$):

$$\nabla \cdot \mathbf{U} = - \underbrace{\frac{1}{C_p} \frac{dC_p}{dt} - \frac{1}{\gamma P} \frac{dP}{dt}}_{(a)} + \underbrace{\frac{\gamma-1}{\gamma P} \left[\frac{4}{3} \mu \left(\frac{\partial W}{\partial z} \right)^2 + \mu \left(\frac{\partial U}{\partial z} \right)^2 \right]}_{(b)} + \underbrace{\frac{\gamma-1}{\gamma P} \frac{\partial}{\partial z} \left(\lambda \frac{\partial T}{\partial z} \right)}_{(c)} + \underbrace{\frac{a^* T}{P} \frac{\partial}{\partial z} \left(\rho D \frac{\partial C}{\partial z} \right)}_{(d)}, \quad (7)$$

where γ is the specific-heat ratio. Assuming that variations in the specific heat can be neglected, Eq. (7) shows that nonzero values of the divergence result from four major sources: (a) Pressure variation (through the coupling with density in the equation of state), (b) viscous dissipation, and (c), (d) molecular diffusion.

In order to better analyze these contributions to the generation of deflection, we define three simplified configurations:

1. *Low-speed binary mixing*, where we consider the mixing of two “incompressible” fluids at the same temperature. The right-hand side of Eq. (7) only involves term (d).
2. *Low-speed thermal mixing*, where we consider temperature mixing without kinetic heating in a single gas, the density of which only depends on temperature. Equation (7) only involves term (c).
3. *High-speed thermal mixing*, where we consider temperature mixing in a single gas with kinetic heating. Equation (7) involves terms (a), (b), and (c).

In the most general case, the physical properties of the fluid depend on the values of the state variables and concentration. A precise definition of the fluid or mixture considered is needed prior to the use of accurate variation laws. In order to be as generic as possible, we shall adopt simple first approximations that will be detailed below for each of the three situations under study.

III. SIMILARITY SOLUTIONS

In this section, we look for self-similar solutions introducing the similarity variable $\eta = z / \delta(t)$, where $\delta(t)$ is some characteristic thickness of the mixing layer at time t . Noting that the boundary conditions when $\eta \rightarrow \pm\infty$ for (ρ, T, U, C) do not depend on t , we look for self-similar solutions of the form

$$\rho = \rho_0 \hat{\rho}(\eta), \quad T = T_0 \hat{\theta}(\eta), \quad U = U_0 \hat{u}(\eta), \quad \text{and} \quad C = \hat{c}(\eta),$$

where ρ_0 , T_0 , and U_0 are constant density, temperature, and velocity characteristic scales, respectively. Conversely, we

introduce the two remaining similarity functions through the following relations:

$$W = W_0(t) \hat{w}(\eta), \quad P - P_\infty = P_0(t) \hat{p}(\eta),$$

where the velocity (W_0) and pressure (P_0) characteristic scales are allowed to vary with time.

Some results, common to the three configurations, can be readily found. If we write the continuity equation (2) and the streamwise momentum equation (3) in their self-similar forms, we get

$$-\frac{\delta}{W_0} \eta \hat{\rho}' + [\hat{\rho} \hat{w}]' = 0, \quad (8)$$

$$-\frac{\delta}{W_0} \eta [\hat{\rho} \hat{u}]' + [\hat{\rho} \hat{w} \hat{u}]' = \frac{\mu}{\rho_0 W_0 \delta} \hat{u}'', \quad (9)$$

where the prime and the dot denote differentiation with respect to η and t , respectively. Self-similarity then requires that $\alpha_1 = \delta / W_0$ and $\alpha_2 = \mu / (\rho_0 W_0 \delta)$ remain constant. The latter can be considered as the inverse of a *reference* Reynolds number (based on the reference quantities W_0 and δ), which should not be confused with the actual transverse Reynolds number (based on the actual width of the layer, and the transverse-velocity amplitude across). In the following, the reference Reynolds number ($1/\alpha_2$) will be given the same value whatever the density ratio and Mach number are, while the actual Reynolds number will vary as a result of the calculations. Now, by subtracting Eq. (8) from Eq. (9) and after simplification, these two equations can be replaced by

$$\hat{\rho}'(-\alpha_1 \eta + \hat{w}) = -\hat{\rho} \hat{w}',$$

$$\hat{\rho} \hat{u}'(-\alpha_1 \eta + \hat{w}) = \alpha_2 \hat{u}''.$$

This form gives immediate information on the extremum of the transverse velocity component: setting \hat{w}' to zero in the first equation, we find that the extremum is located at a value of η such that

$$\eta = \hat{w}(\eta) / \alpha_1. \quad (10)$$

When this result is injected in the second equation, it appears that $u''(\eta)$ is simultaneously zero. In other words, *maximum deflection* coincides with the inflection point of the (longitudinal) velocity profile. Equation (10) also shows that the velocity profile—referenced with the location of its inflection point—does not remain centered: the shift from the origin amounts to

$$\hat{w}_{\max} \delta / \alpha_1,$$

or equivalently,

$$W_{\max} \delta / \dot{\delta}.$$

From the first expression, we conclude that the shift increases at the same rate as δ and appears, therefore, as a *continuous time drift of the shear layer*. The second expression shows that its direction follows directly from that of the deflection—since $\delta / \dot{\delta}$ is obviously positive.

A relation similar to Eq. (10) was obtained by Pantano and Sarkar⁶ in the self-similar analysis of the turbulent case. Note, however, that the drift was not defined with reference to the inflection point of the velocity profile, but to the point of zero velocity. Pantano and Sarkar⁶ also indicated that the drift is always directed toward the light fluid—a conclusion that will be confirmed below for our case, but that we cannot draw at this stage.

A. Low-speed binary mixing

The first case under study is the isothermal mixing of two incompressible fluids. In this situation, the only source of deflection comes from molecular mass transfer. At this stage, we have to introduce some assumptions regarding the physical properties of the mixture. First, we note that, according to the Chapman-Enskog formula (see, for example, Bird, Stewart, and Lightfoot¹³), the mass-diffusivity coefficient D does not depend on concentration. Second, according to Wilke’s formula (see also Bird, Stewart, and Lightfoot¹³), the viscosity μ of the mixture depends mainly on temperature and only loosely on concentration. We shall therefore assume that both diffusion coefficients are constant in our problem (as well as their ratio given by the *global* Schmidt number $Sc = \mu \rho_0^{-1} D^{-1}$).

Now, the mass fraction C of fluid A can be linked to the density of the mixture, and the equation of state (1) simplifies to

$$\rho = \frac{\rho_A - \rho_B}{\rho_A} \rho C + \rho_B.$$

This equation together with Eqs. (2)–(5) fully define the problem. Introducing the Atwood number $\mathcal{A} = (\rho_B - \rho_A) / (\rho_B + \rho_A)$ and setting ρ_0 to $(\rho_B + \rho_A) / 2$, the self-similar form of the governing system can be written as

$$\hat{\rho}(2\mathcal{A}\hat{c} + 1 - \mathcal{A}) = 1 - \mathcal{A}^2, \tag{11}$$

$$-\alpha_1 \eta \hat{\rho}' + [\hat{\rho}\hat{w}]' = 0, \tag{12}$$

$$-\alpha_1 \eta [\hat{\rho}\hat{c}]' + [\hat{\rho}\hat{w}\hat{c}]' = \alpha_2 [\hat{\rho}Sc^{-1}\hat{c}]', \tag{13}$$

$$-\alpha_1 \eta [\hat{\rho}\hat{u}]' + [\hat{\rho}\hat{w}\hat{u}]' = \alpha_2 \hat{u}'', \tag{14}$$

TABLE I. Initial and boundary conditions for the self-similarity analysis [with $\mathcal{A} = (\rho_B - \rho_A) / (\rho_B + \rho_A)$, $T_0 = (T_B + T_A) / 2$, and $\rho_0 = (\rho_B + \rho_A) / 2$].

Variable	Boundary conditions		Initial conditions	
	$z \rightarrow -\infty$	$z \rightarrow +\infty$	$z < 0$	$z > 0$
\hat{c}	1	0	1	0
$\hat{\theta}$	$1 + \mathcal{A}$	$1 - \mathcal{A}$	$1 + \mathcal{A}$	$1 - \mathcal{A}$
$\hat{\rho}$	$1 - \mathcal{A}$	$1 + \mathcal{A}$	$1 - \mathcal{A}$	$1 + \mathcal{A}$
\hat{u}	-1	1	-1	1
\hat{w}	$\hat{w}' = 0$	$\hat{w}' = 0$	0	0

$$-\alpha_1 \eta [\hat{\rho}\hat{w}]' + [\hat{\rho}\hat{w}^2]' + \alpha_3 \hat{\rho}\hat{w} = \frac{4}{3} \alpha_2 \hat{w}'' - \alpha_4 \hat{\rho}', \tag{15}$$

with $\alpha_3 = \delta \dot{W}_0 / W_0^2$ and $\alpha_4 = P_0 / (\rho_0 W_0^2)$. It is to be solved subject to the boundary conditions given in Table I. It is now required that $\alpha_1 - \alpha_4$ be constants, which gives the time-dependent characteristic scales of the problem in the following forms:

$$\delta(t) = \sqrt{2 \frac{\mu}{\rho_0} \frac{\alpha_1}{\alpha_2} t}, \quad W_0(t) = \sqrt{\frac{\mu}{2\rho_0 \alpha_1 \alpha_2} t^{-1}}, \tag{16}$$

and

$$P_0(t) = \frac{\mu \alpha_4}{2 \alpha_1 \alpha_2} t^{-1}. \tag{17}$$

The values of the α coefficients can be chosen arbitrarily, provided that α_1 and α_2 have the same sign, and that $\alpha_3 = -\alpha_1$. From Eqs. (16) and (17), we can conclude that the width of the mixing layer increases as the square root of time, while the amplitude of the deflection decreases as its inverse.

In order to proceed with the solution of the spatial problem, we notice that Eqs. (11)–(13) can be solved for $(\hat{\rho}, \hat{c}, \hat{w})$ independently of Eqs. (14) and (15). Using Eq. (11) to write \hat{c} as a function of $\hat{\rho}$, substituting this expression in Eq. (15), and subtracting Eq. (8), we find

$$\hat{w}' + \frac{\alpha_2}{Sc} \left[\frac{\hat{\rho}'}{\hat{\rho}} \right]' = 0 \Leftrightarrow \hat{w} + \frac{\alpha_2 \hat{\rho}'}{Sc \hat{\rho}} = \text{const.}$$

Obviously, the constant must be zero in order to satisfy the initial conditions at infinity. We can then write $\hat{\rho}\hat{w} = -\alpha_2 \hat{\rho}' / Sc$ and inject this quantity into Eq. (8) to find

$$\alpha_1 \eta \hat{\rho}' + \frac{\alpha_2}{Sc} \hat{\rho}'' = 0. \tag{18}$$

Integration is straightforward; the expressions of \hat{w} and \hat{c} follow. Integration of Eq. (15) can then be easily performed to give the solution for $\hat{\rho}$. Taking, arbitrarily,

$$\alpha_1 = 2, \quad \alpha_2 = Sc, \quad \alpha_3 = -2, \quad \text{and} \quad \alpha_4 = 1,$$

the final expressions read

$$\hat{\rho} = 1 + \mathcal{A} \operatorname{erf} \eta, \tag{19}$$

$$\hat{w} = -\frac{2\mathcal{A}}{\sqrt{\pi}} \frac{\exp(-\eta^2)}{1 + \mathcal{A} \operatorname{erf} \eta}, \tag{20}$$

$$\hat{c} = \frac{1 - \mathcal{A}}{2} \frac{1 - \operatorname{erf} \eta}{1 + \mathcal{A} \operatorname{erf} \eta}, \tag{21}$$

$$\begin{aligned} \hat{\rho} = & -\frac{4\mathcal{A}}{\sqrt{\pi}} \eta \exp(-\eta^2) - \frac{4\mathcal{A}^2}{\pi} \frac{\exp(-2\eta^2)}{1 + \mathcal{A} \operatorname{erf} \eta} \\ & + Sc \frac{16\mathcal{A}}{3\pi} \frac{\exp(-\eta^2)}{(1 + \mathcal{A} \operatorname{erf} \eta)^2} \\ & \times [\sqrt{\pi} \eta (1 + \mathcal{A} \operatorname{erf} \eta) + \mathcal{A} \exp(-\eta^2)]. \end{aligned} \tag{22}$$

Unfortunately, a closed-form solution for \hat{u} is not obvious, and numeric integration of Eq. (14) will be needed to obtain the evolution of the longitudinal velocity component.

B. Low-speed thermal mixing

We now consider the mixing layer between two flows of the same fluid with different temperatures. We assume that the dissipation can be neglected (low Mach number) and that the density of the fluid only depends on the temperature (purely dilatable gas). The only source for flow divergence is now viscous diffusion. Usually, the viscosity μ and thermal diffusivity λ both depend on temperature, their ratios—proportional to the Prandtl number $\text{Pr} = \mu C_p / \lambda$ —remaining approximately constant. However, we shall consider for simplicity that both diffusivities remain constant.

In this situation, we use the following equation of state:

$$\rho T = \rho_A T_A = \rho_B T_B.$$

Setting T_0 to $(T_A + T_B)/2$, the self-similar form of the governing system becomes

$$\hat{\rho} \hat{\theta} = 1 - \mathcal{A}^2, \quad (23)$$

$$- \alpha_1 \eta \hat{\rho}' + [\hat{\rho} \hat{w}]' = 0, \quad (24)$$

$$- \alpha_1 \eta [\hat{\rho} \hat{\theta}]' + [\hat{\rho} \hat{w} \hat{\theta}]' = \alpha_2 [\text{Pr}^{-1} \hat{\theta}']', \quad (25)$$

$$- \alpha_1 \eta [\hat{\rho} \hat{u}]' + [\hat{\rho} \hat{w} \hat{u}]' = \alpha_2 \hat{u}'', \quad (26)$$

$$- \alpha_1 \eta [\hat{\rho} \hat{w}]' + [\hat{\rho} \hat{w}^2]' + \alpha_3 \hat{\rho} \hat{w} = \frac{4}{3} \alpha_2 \hat{w}'' - \alpha_4 \hat{\rho}'. \quad (27)$$

It is to be solved subject to the boundary conditions given in Table I, and with the same definitions of the α coefficients as in the previous case. The time-dependent characteristic scales of this problem are thus still given by relations (16) and (17).

Here again, we notice that the subsystem (23)–(25) can be solved independently. With the same kind of algebra as in Sec. III A, we can obtain a simple differential equation for the density,

$$\alpha_1 \eta \hat{\rho}' + \frac{\alpha_2}{\text{Pr}} \left[\frac{\hat{\rho}'}{\hat{\rho}} \right]' = 0. \quad (28)$$

This equation is the analog of Eq. (18), obtained in the previous case. The main difference comes from the fact that the Prandtl number is a constant, whereas, in the case of binary mixing, its equivalent (the local Schmidt number $\sigma_c = \text{Sc} / \hat{\rho}$) varies as the inverse of the density. This difference prevents one from giving a closed-form solution to Eq. (28). However, the solutions for $\hat{\theta}$, \hat{w} , and \hat{p} directly follow from the solution for $\hat{\rho}$: Taking

$$\alpha_1 = 2, \quad \alpha_2 = \text{Pr}, \quad \alpha_3 = -2, \quad \text{and} \quad \alpha_4 = 1$$

(the same as above except for α_2), we find that

$$\hat{\theta} = \frac{1 - \mathcal{A}^2}{\hat{\rho}}, \quad \hat{w} = - \frac{\hat{\rho}'}{\hat{\rho}^2}, \quad (29)$$

and

$$\hat{p} = 2 \eta \hat{\rho} \hat{w} - \hat{\rho} \hat{w}^2 + \frac{4 \text{Pr}}{3} \hat{w}', \quad (30)$$

while the determination of the longitudinal velocity component still needs a numeric integration of Eq. (26).

C. High-speed thermal mixing

In the last case under study, we again consider the mixing layer between two flows of the same fluid and different temperatures, but the longitudinal velocity component is now high enough for kinetic heating to be significant. It follows that the dependence of the density on pressure cannot be neglected *a priori*, and all the possible sources of divergence for a single gas must be considered.

Still assuming that both the viscosity μ and thermal diffusivity λ do not depend on temperature, and using the ideal-gas equation of state $P = \rho \mathcal{R} T$, the governing system can be cast under the following self-similar form:

$$\begin{aligned} \hat{\rho} \hat{\theta} &= 1 - \mathcal{A}^2 + \alpha_4 \gamma M_w^2 \hat{\rho}, \\ - \alpha_1 \eta \hat{\rho}' + [\hat{\rho} \hat{w}]' &= 0, \\ - \alpha_1 \eta [\hat{\rho} \hat{\theta}]' + [\hat{\rho} \hat{w} \hat{\theta}]' &= \alpha_2 \gamma [\text{Pr}^{-1} \hat{\theta}']' - (\gamma - 1) \hat{\rho} \hat{\theta} \hat{w}' \\ &\quad + \alpha_2 \gamma (\gamma - 1) \left(M_u^2 \hat{u}'^2 + \frac{4}{3} M_w^2 \hat{w}'^2 \right), \\ - \alpha_1 \eta [\hat{\rho} \hat{u}]' + [\hat{\rho} \hat{w} \hat{u}]' &= \alpha_2 \hat{u}'', \\ - \alpha_1 \eta [\hat{\rho} \hat{w}]' + [\hat{\rho} \hat{w}^2]' + \alpha_3 \hat{\rho} \hat{w} &= \frac{4}{3} \alpha_2 \hat{w}'' - \frac{\alpha_1}{\gamma M_w^2} \hat{\rho}', \end{aligned}$$

where the energy equation has been taken under its internal-energy form, and the longitudinal and transverse Mach numbers are defined by

$$M_u^2 = \frac{U_0^2}{\gamma \mathcal{R} T_0} \quad \text{and} \quad M_w^2 = \frac{W_0^2}{\gamma \mathcal{R} T_0}.$$

With our definitions of the characteristic temperature and streamwise velocity scales, M_u corresponds to the convective Mach number. Self-similarity now requires that both Mach numbers remain constant, as well as the previously defined α coefficients. Taking M_w and α_1 as constants leads to $\delta = \text{const}$, which is obviously unacceptable. We can thus conclude that there is no general self-similar solution to this problem. However, considering that the transverse velocity should be small as compared to the speed of sound, we shall study the limiting case in which M_w goes to zero. The conditions on the α coefficients then lead to evolutions of the time-dependent characteristic scales, which are similar to relations (16) and (17). These are rewritten in the form

$$\delta = \left[\delta_1^2 + \frac{2 \mu \alpha_1}{\rho_0 \alpha_2} (t - t_1) \right]^{1/2}, \quad (31)$$

$$P_0 = \alpha_4 \left[\frac{1}{\rho_0 W_1^2} + \frac{2 \alpha_1 \alpha_2}{\mu} (t - t_1) \right]^{-1}, \quad (32)$$

$$W_0 = \left[\frac{1}{W_1^2} + \frac{2\rho_0\alpha_1\alpha_2}{\mu}(t-t_1) \right]^{-1/2}, \quad (33)$$

where δ_1 is the characteristic thickness of the mixing layer at time t_1 and $W_1 = \mu/(\rho_0\delta_1\alpha_2)$. Introduction of the reference at $t=t_1$ follows from the fact that, according to relation (33), the value of W_0 can be seen to decrease as time proceeds. The hypothesis on the transverse Mach number will therefore be satisfied for $t > t_1$ if t_1 is sufficiently large, and our solution appears to approximate the evolution of the high-speed thermal mixing layer at large times. In this regime, the transverse momentum equation reduces to $\hat{p}'=0$, and the self-similar form of the governing system becomes

$$\hat{\rho}\hat{\theta} = 1 - \mathcal{A}^2 \quad (\equiv \hat{p}), \quad (34)$$

$$-\alpha_1\eta\hat{\rho}' + [\hat{\rho}\hat{w}]' = 0, \quad (35)$$

$$\alpha_2[\text{Pr}^{-1}\hat{\theta}'] - (1 - \mathcal{A}^2)\hat{w}' = -\alpha_2(\gamma - 1)M_u^2\hat{u}'^2, \quad (36)$$

$$-\alpha_1\eta[\hat{\rho}\hat{u}]' + [\hat{\rho}\hat{w}\hat{u}]' = \alpha_2\hat{u}'' \quad (37)$$

A solution to these equations along with the boundary conditions given in Table I cannot be obtained in closed form. However, some information on the deflection is available at this stage: Integrating Eq. (36) across the layer, and assuming that the temperature gradients vanish when η goes to $\pm\infty$, leads to

$$\hat{w}_B - \hat{w}_A = \alpha_2 \frac{\gamma - 1}{1 - \mathcal{A}^2} M_u^2 \int_{-\infty}^{+\infty} \hat{u}'^2 d\eta. \quad (38)$$

The right-hand side of this relation cannot be zero as soon as M_u is nonzero. As a consequence, \hat{w}_B is necessarily higher than \hat{w}_A , the difference being proportional to the total amount of dissipation in the flow. The physical mechanism at work is easy to understand: Overheating in the core of the mixing layer is responsible for the dilatation of the fluid there, and subsequent generation of transverse velocity toward the outer parts of the flow. Transport by this transverse velocity component should contribute to the growth rate of the mixing layer—which usually results from purely diffusive transport. We shall refer to this effect as *advective growth* in the following. Note that advective growth should not be confused with entrainment (observed in space-evolving mixing layers.)

The integral constraint (38) further shows that the transverse velocity component cannot be simultaneously zero at $\eta = \pm\infty$. Moreover, it can be readily seen that changing \hat{w} into $\hat{w} + w_0$ and η to $\eta + w_0/\alpha_1$ leaves the system (34)–(37) unchanged whatever the (constant) value of w_0 is. Since the solution is only valid at large times, we do not have any reason to choose one value or another for w_0 (such a value should be deduced from the initial condition), and we shall impose without any loss of generality that $\hat{w}_A = -\hat{w}_B$.

IV. RESULTS

In order to fully solve the three self-similar problems presented in the preceding section, we need to resort to variable amounts of numeric integration:

- of Eq. (14), for the case of binary mixing;
- of Eqs. (28) and (26), for the case of low-speed thermal mixing;
- of Eqs. (34)–(37), for the case of high-speed thermal mixing.

These ordinary differential equations are discretized using second-order finite-difference schemes, and then iterated until convergence. The size of the computational domain is roughly twice that of the mixing layer, and we use 600 points across the full domain (half that number of points gives virtually the same results). The calculations have been performed with

$$\text{Pr} = \text{Sc} = 0.7 \quad \text{and} \quad \gamma = 1.4.$$

The values adopted for the Prandtl number and specific-heat ratio are those applicable to air at the temperature and pressure normal conditions. For the Schmidt number, a value of order unity—applicable to ordinary gaseous mixtures—has been chosen. We have further set $\text{Pr}=\text{Sc}$ in order to keep the same definitions of the time-dependent characteristic scales in either binary and thermal mixing, and ease the comparison between the two cases.

The evolutions of the main flow quantities are reviewed in the following paragraphs for the three configurations under study.

A. Transverse velocity component

The most specific feature of the variable-density mixing layer is flow deflection. For this reason, we start with an examination of the transverse component of the velocity profile in Fig. 1. For each of the three configurations, the profiles are plotted for a wide range of density ratios $\rho_B/\rho_A = 1, 3, 7, 15, 31$ (corresponding to $\mathcal{A}=0, 0.5, 0.75, 0.875, 0.9375$) in Figs. 1(a)–1(c).

In the cases of low-speed binary and thermal mixing, the deflected region is (asymptotically) confined in the center of the mixing layer, and the effect of the density ratio is to increase its extent as well as the value of the deflection. As indicated by Eqs. (20) and (29), deflection is directed toward the light side of the flow. Moreover, the thickening of the deflected region when \mathcal{A} increases seems to occur at the light edge of this region. This can be explained in the case of binary mixing by setting \mathcal{A} to unity (its maximum value) in the exact solution (20). The resulting expression,

$$\hat{w} = -\frac{2}{\sqrt{\pi}} \frac{\exp(-\eta^2)}{1 + \text{erf } \eta}, \quad (39)$$

is singular toward the light side of the flow ($\eta \rightarrow -\infty$), but remains defined above where it constitutes the limiting curve for the velocity profiles when the density ratio increases. One can observe the same kind of behavior in the case of low-

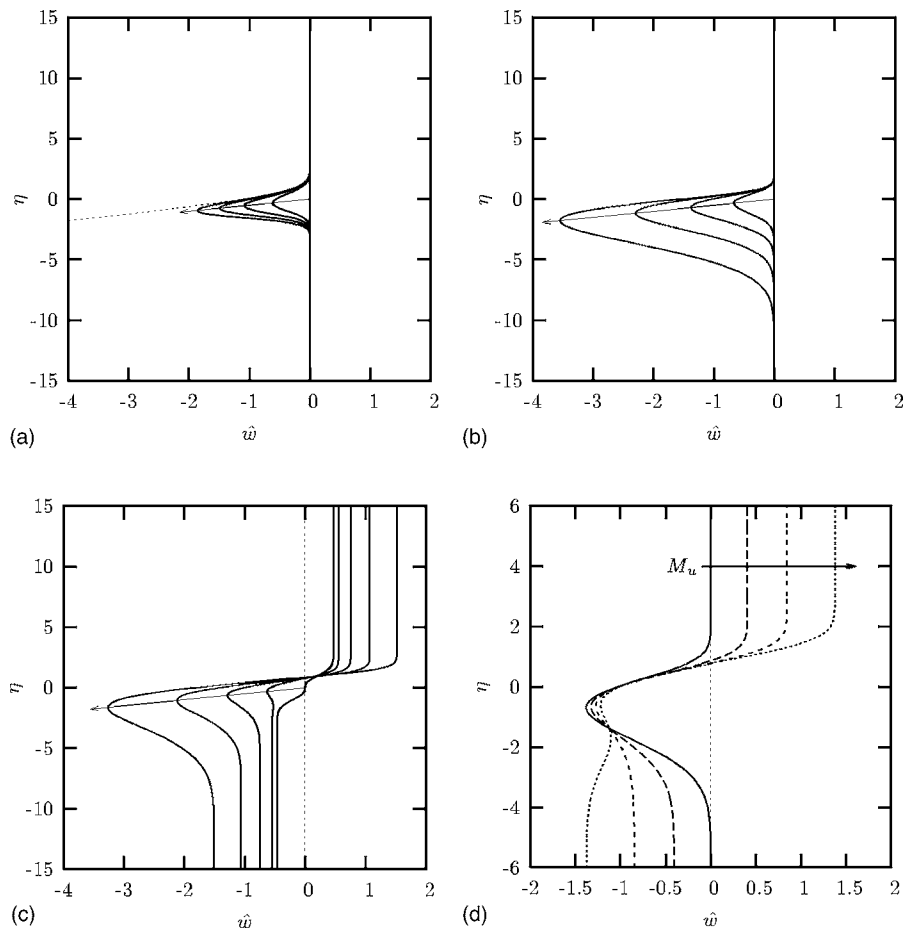


FIG. 1. Profiles of the transverse velocity component across the mixing layer. (a) Low-speed binary mixing, (b) low-speed thermal mixing, and (c) high-speed thermal mixing at $M_u = 1.4$, with different values of the Atwood number. $\mathcal{A} = 0, 0.5, 0.75, 0.875, 0.9375$. On each plot, the arrow indicates increasing values of \mathcal{A} and connects the points of maximum deflection in agreement with relation (10); the dashed line in plot (a) corresponds to Eq. (39). (d) High-speed thermal mixing with $\mathcal{A} = 0.75$ and different values of the Mach number: $M_u = 0, 1, 1.5, 2$.

speed thermal mixing, but an exact expression of the limiting curve cannot be given in this configuration.

In the case of high-speed thermal mixing [Fig. 1(c)], a *global deflection* is superimposed onto the “local” deflection observed in the low-speed cases. It is apparent on the plots from the nonzero asymptotic values of the velocity as $\eta \rightarrow \pm\infty$, while the “local” deflection [of diffusive nature, see terms (c) and (d) of Eq. (7)] can still be observed in the negative- η region with a local maximum oriented toward the light side of the flow. In agreement with its dilatational origin, the global deflection is oriented from the center of the layer toward the upper and lower free streams. Interestingly, it is amplified by an increase in the density ratio, even if the value of the Mach number remains constant. This is obviously due to the presence of the term $(1 - \mathcal{A}^2)$ in the right-end side of Eq. (38).

The transverse velocity profiles obtained for different values of the Mach number and the same value of the Atwood number have been plotted in Fig. 1(d). The increase of the global deflection with increasing Mach number is apparent. A slight decrease in the maximum of the “diffusive” deflection can be observed at the same time so that (for $\mathcal{A} = 0.75$ and $M_u = 2$ for instance) the velocity profile can experience a local minimum at the light side of the flow, the absolute value of the deflection being higher in the free stream than in the center of the layer.

B. Density

The density profiles obtained in the case of binary mixing and different values of the Atwood number are plotted in Fig. 2(a). They are centered at $\eta = 0$ and symmetric across the mixing layer, in agreement with the exact solution (19).

These properties are lost in the case of low-speed thermal mixing [see Fig. 2(b)]. The profiles seem to drift toward the heavy side of the flow, the drift being enhanced with increasing values of the Atwood number. The self-similar equations can be used to confirm this observation: Setting ρ' to zero in Eq. (28) and using the expression of w as a function of ρ in Eq. (29) leads to $\eta = -\hat{w}/2$ at the inflection point of the density profile. Since \hat{w} is negative everywhere in the mixing layer, we can conclude that η is positive at the inflection point of the density profile. On the other hand, the loss of symmetry is easy to understand considering that the product $\text{Pr}^{-1}\hat{\rho}^{-1}$ acts as a diffusion coefficient in Eq. (28) and, therefore, increases with decreasing $\hat{\rho}$. Consistently, the density profile appears as “smoother” toward the light edge of the mixing layer.

In the case of high-speed thermal mixing [Fig. 2(c)], the same observations can be made. The drift of the density profile is still present, but significantly enhanced by advective growth. (The inflection point of the density profile is moved slightly above the axis, maximum heat release due to dissipation coinciding with the inflection point of the velocity

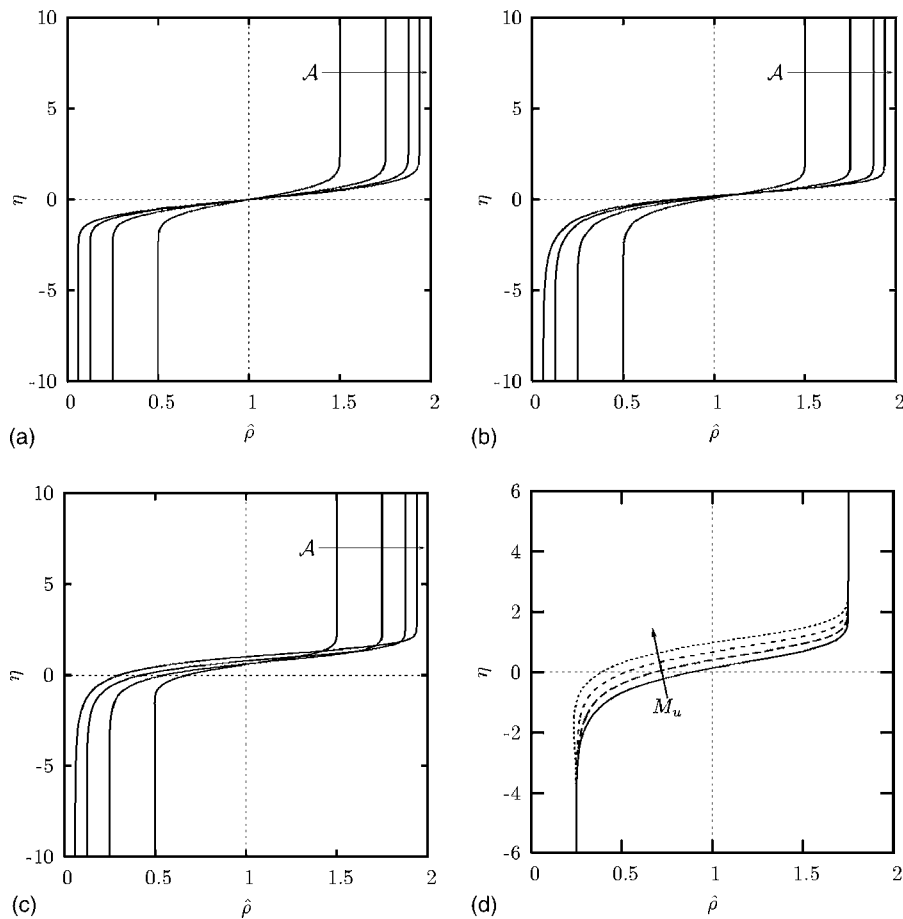


FIG. 2. Density profiles across the mixing layer. (a) Low-speed binary mixing, (b) low-speed thermal mixing, and (c) high-speed thermal mixing at $M_u=1.4$, with different values of the Atwood number. $\mathcal{A}=0.5, 0.75, 0.875, 0.9375$. (d) High-speed thermal mixing with $\mathcal{A}=0.75$ and different values of the Mach number: $M_u=0, 1, 1.5, 2$.

profile, i.e., well below the axis.) The Mach-number effect can be examined in Fig. 2(d). The drift of the profile is enhanced when the Mach number increases; this is obviously due to increasing advective growth.

C. Concentration and temperature

In order to compare the binary and thermal mixing configurations, we introduce a new similarity variable \tilde{c} derived from the concentration and such that

$$\tilde{c} = 2\mathcal{A}\hat{c} + 1 - \mathcal{A}.$$

This “pseudo” concentration plays strictly the same role in the equation of state (11) for binary mixing as the temperature in the equation of state (23) for low-speed thermal mixing. Moreover, an equation for \tilde{c} is easily derived from Eq. (13), which has the same structure as Eq. (25) for $\hat{\theta}$ (except for the difference in diffusion coefficients already mentioned). Finally, note that \tilde{c} and $\hat{\theta}$ share the same boundary conditions:

$$\tilde{c}(-\infty) = \hat{\theta}(-\infty) = 1 + \mathcal{A}$$

and

$$\tilde{c}(+\infty) = \hat{\theta}(+\infty) = 1 - \mathcal{A}.$$

All of this is an incitement to compare the pseudoconcentration and temperature profiles, as we do in Fig. 3.

When the pseudoconcentration profiles obtained in the case of binary mixing [Fig. 3(a)] and the temperature profiles obtained in the case of low-speed thermal mixing [Fig. 3(b)] are considered, it appears that all of them drift toward the light edge of the mixing layer. As for the other flow quantities, the drift is increased with increasing Atwood numbers. With the same kind of algebra as that used for the density profiles, it is a simple matter to show that the inflection point of the concentration profile is located at a value of η such that $\eta = \hat{w}$, and that the inflection point of the temperature profile is located at η such that $\eta = \hat{w}/2$. Both values are obviously negative and increase in magnitude with the Atwood number (since the transverse velocity does). On the other hand, the variations in the width of the mixing layer with increasing Atwood number appear as fairly different in the two cases. In the case of thermal mixing, the width of the layer increases significantly as the Atwood number increases. The way this thickening proceeds—mainly at the light edge of the layer—is reminiscent of the evolution of the transverse velocity component, so that the thickening of the mixing region can most presumably be attributed to increased deflection. In the case of binary mixing, the deflection also increases with the Atwood number. In this case, however, the diffusion coefficient for concentration is proportional to density [see Eq. (5)], so that diffusion at the light edge decreases as the Atwood number increases. As a result, the effect of

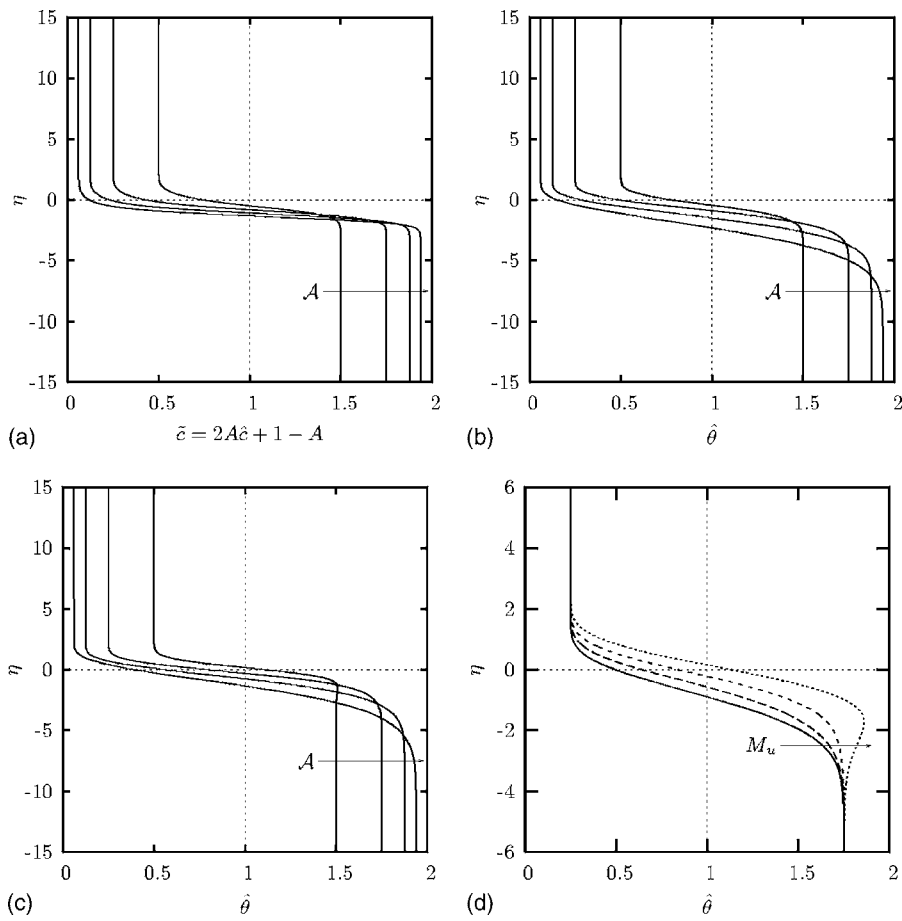


FIG. 3. Concentration or temperature profiles across the mixing layer. (a) Low-speed binary mixing, (b) low-speed thermal mixing, and (c) high-speed thermal mixing at $M_u=1.4$, with different values of the Atwood number. $A=0.5, 0.75, 0.875, 0.9375$. (d) High-speed thermal mixing with $A=0.75$ and different values of the Mach number: $M_u=0, 1, 1.5, 2$.

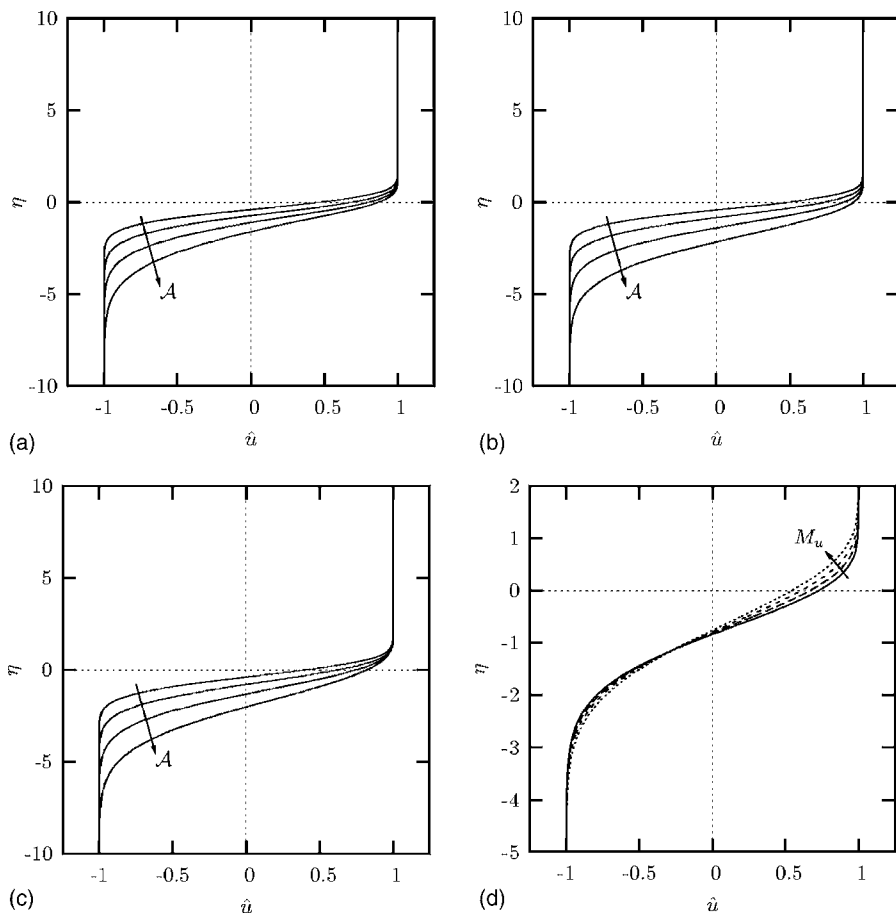


FIG. 4. Profiles of the longitudinal velocity component across the mixing layer. (a) Low-speed binary mixing, (b) low-speed thermal mixing, and (c) high-speed thermal mixing at $M_u=1.4$, with different values of the Atwood number. $A=0.5, 0.75, 0.875, 0.9375$. (d) High-speed thermal mixing with $A=0.75$ and different values of the Mach number: $M_u=0, 1, 1.5, 2$.

reduced diffusion counteracts the effect of increased deflection and the width of the layer barely varies (actually decreases, see Sec. IV F).

As compared to the low-speed case, the shift observed in the situation of high-speed thermal mixing seems to be reduced [Fig. 3(c)], it even appears to be positive for $\mathcal{A}=0.5$ and $M_u=1.4$. This is a direct consequence of the overheating by viscous dissipation that takes place in the middle of the mixing layer. This phenomenon is well evidenced in Fig. 3(d), which shows that, with the same value of the Atwood number, increasing the Mach number leads to the appearance of a local maximum and a reduction of the observed drift.

D. Streamwise velocity component

The profiles of the longitudinal velocity component across the flow are plotted in Fig. 4 for the three configurations and different Atwood and Mach numbers. In the case of a constant-density mixing layer, the velocity profiles should be centered and symmetrical. Both properties are lost in the three configurations of variable-density mixing layers studied here. In agreement with the similarity analysis, the profiles can be seen to drift more and more toward the light side of the flow with increasing Atwood numbers. Also obvious in the figure is the thickening of the shear layer at the same time. As previously observed from the temperature profiles, this thickening occurs mainly at the light edge of the layer, and likely results from increased deflection. Finally, the

Mach-number effect can be observed in Fig. 4(d): increasing the value of this number also leads to a moderate thickening of the shear layer.

E. Streamlines

Plots of the streamlines obtained at any time in the three configurations under study are presented in Fig. 5. The presence of a *deflected layer* in the low-speed configurations, as well as that of a *global flow deflection* in the high-speed configuration, are the most striking features of these plots. Another important point is that, for all three configurations and as soon as the Atwood number is nonzero, one can observe that heavy fluid is deflected toward the light side of the flow before being entrained backwards with the lower free stream. In a time-dependent flow like this, streamlines are indeed not fully representative of the real flow motion; however, we have calculated the trajectories of the fluid particles, and the plots (not reported here) definitely confirm such a change in the direction of the flow motion. Note also that, in the low-speed cases, all the initially heavy fluid particles will experience such a change in their flow direction at more or less long term. On the other hand, when kinetic heating is present, Fig. 5(c) shows that this phenomenon only applies to a limited region of the initially heavy fluid, comprised between $\eta=0$ and the point where \hat{w} changes sign. Figure 1(c) showed that this point is located above the x axis, rises up with increasing Atwood number, but obviously reaches some

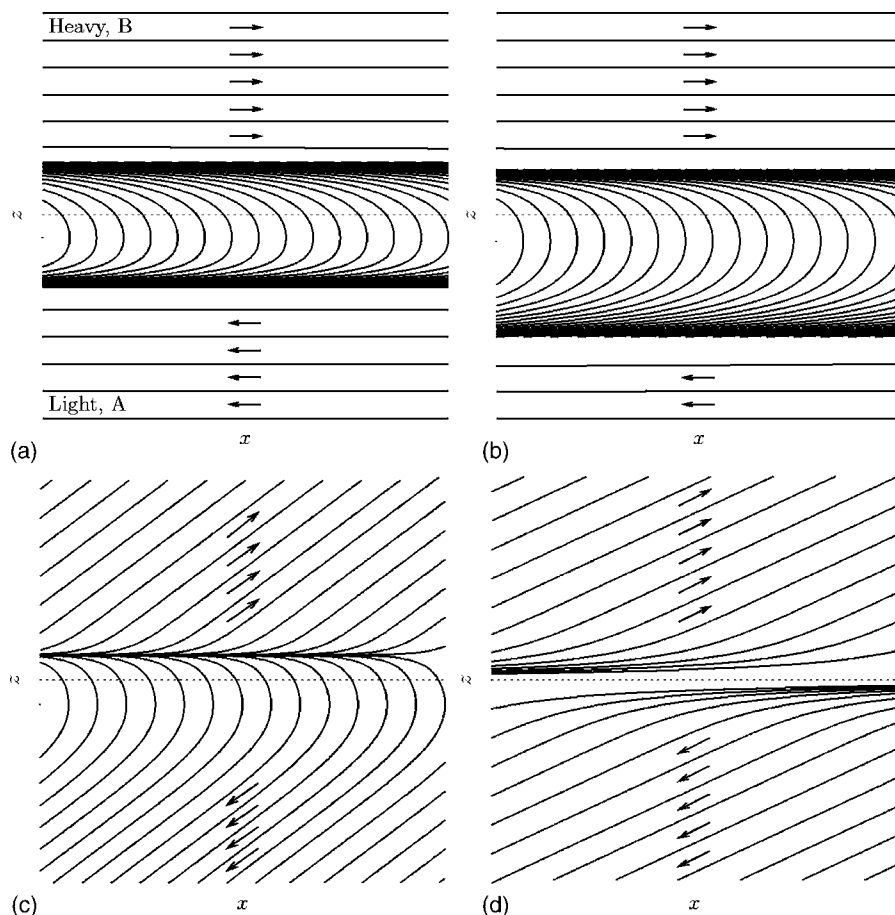


FIG. 5. Instantaneous streamlines in the mixing layer. (a) Low-speed binary mixing with $\mathcal{A}=0.75$, (b) low-speed thermal mixing with $\mathcal{A}=0.75$, (c) high-speed thermal mixing with $\mathcal{A}=0.75$ and $M_u=1.4$, and (d) high-speed thermal mixing with $\mathcal{A}=0$ and $M_u=1.4$. The dotted line corresponds to the $z=0$ axis, and the scale ratio between the x and z axis is arbitrary.

finite limit [the highest value of the Atwood number used in Fig. 1(c) is about 0.94, which correspond to a density ratio as high as 31]. A consequence of these observations is that the notion of *dividing streamline* for variable-density mixing layers can be considered as meaningful *only* if kinetic heating is present. Moreover, in this case, it does not delimit the initially heavy fluid from the lighter one, but only some part of it.

The global deflection associated with kinetic heating can be observed in Figs. 5(c) and 5(d), where it is evidenced by a “tilting” of the velocity field (especially apparent in the free stream.) Comparison of Figs. 5(c) and 5(d), where the Mach number is the same and the Atwood number has been set to zero in the latter, illustrates that the global deflection is reduced with decreasing Atwood numbers. Such tilts obviously arise from the choice $\hat{u}_B = -\hat{u}_A (=1)$ and $\hat{w}_B = -\hat{w}_A (= \Delta w/2)$, and one may wonder how the global deflection would appear in a coflowing mixing layer with $\hat{u}_B > \hat{u}_A > 1$. The question can be answered by considering the translational invariances of the problem: As stated in Sec. III C, the coflowing mixing layers defined by

$$\hat{u}_B = u_c + 1, \quad \hat{u}_A = u_c - 1$$

and

$$\hat{w}_B = w_0 + \Delta w/2, \quad \hat{w}_A = w_0 - \Delta w/2,$$

with $u_c > 1$, are strictly equivalent to those computed above whatever the value of w_0 is. Now, taking $w_0 = u_c \Delta w/2$ cancels the “tilting” of the velocity field in the high-speed thermal mixing case since, with such a choice, $\hat{w}_B/\hat{u}_B = -\hat{w}_A/\hat{u}_A$. The corresponding streamline pattern is plotted in Fig. 6 for the same flow as that illustrated in Fig. 5(d). One can see that the dividing streamline has moved toward the light side of the layer, thus indicating a *global* drift of the mixing/shear layer as time goes on [given by a fixed fraction of $\delta(t)$]. As a conclusion, we can consider that the global deflection observed in high-speed thermal mixing can manifest itself either by a tilting of the velocity field or by a global drift of the

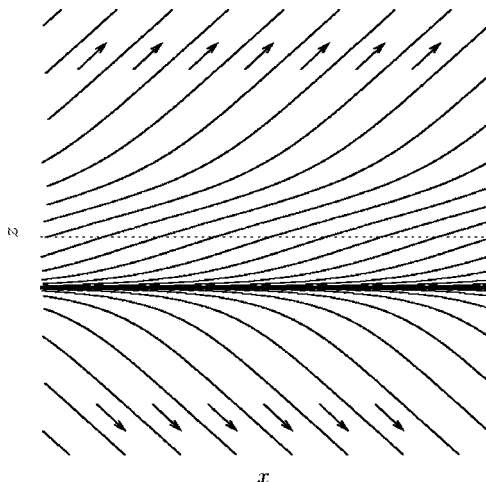


FIG. 6. Instantaneous streamlines in the coflowing mixing layer ($\hat{u}_c=3$). High-speed thermal mixing with $\mathcal{A}=0$ and $M_u=1.4$. The dotted line corresponds to the $z=0$ axis, and the scale ratio between the x and z axis is arbitrary.

layer. Hence, it can be conjectured that the drift toward the light side of the flow observed in space-evolving mixing layers could be a combination of this global drift (Mach-number effect) and the drift between the density and longitudinal-velocity profiles (mixing effect).

F. Density-ratio and Mach-number effects

In this section, we are interested in the influences of the density ratio and Mach number on the time evolution of the mixing layer. The vorticity and momentum thicknesses (δ_ω and δ_θ) are commonly used to study the spreading rate of the *shear* layer. They are defined by

$$\delta_\omega = 2U_0 \left. \frac{\partial U}{\partial z} \right|_{\max}^{-1}$$

and

$$\delta_\theta = \frac{1}{4\rho_0 U_0^2} \int_{-\infty}^{+\infty} \rho(U_0 + U)(U_0 - U) dz.$$

Introducing the similarity variables and taking the time derivatives of these quantities give the expressions of the corresponding spreading rates,

$$\dot{\delta}_\omega = \dot{\delta} \times \frac{2}{\hat{u}'_{\max}} \quad \text{and} \quad \dot{\delta}_\theta = \dot{\delta} \times \frac{1}{4} \int_{-\infty}^{+\infty} \hat{\rho}(1 - \hat{u}^2) d\eta.$$

As *mixing* is concerned, we also introduce conventional thicknesses based on the concentration and temperature profiles: δ_C and δ_T . These are defined as the distance between the points where the concentration goes from 0.1 to 0.9 for the former, and between the points where the temperature goes from $T_A - 0.1(T_A - T_B)$ to $T_A - 0.9(T_A - T_B)$ for the latter. The corresponding expressions of the spreading rates can be written as

$$\dot{\delta}_C = \dot{\delta} \times (\eta_{C=0.9} - \eta_{C=0.1})$$

and

$$\dot{\delta}_T = \dot{\delta} \times (\eta_{\theta=1-0.8A} - \eta_{\theta=1+0.8A}).$$

The spreading rates normalized by their constant-density value are plotted against the density ratio in Fig. 7 for the situations of low-speed binary and thermal mixing. In both cases, the momentum thickness can be seen to decrease with increasing values of the density ratio. The spreading rates based on the conventional (nonintegral) thicknesses exhibit a different behavior: While those based on the vorticity and temperature increase with the density ratio, the spreading rate based on the concentration decreases. This result confirms the conclusion drawn from the inspection of the concentration and temperature profiles in Sec. IV C, according to which the difference in the behaviors of the spreading rates should be attributed to the form of the diffusion coefficients: constant for the velocity and temperature, and proportional to density for the concentration.

Also plotted in Fig. 7 is a measure of the shear-layer drift. This quantity is denoted as h and defined as the distance between the inflection points of the density and velocity profiles. In the case of binary mixing, the density profile

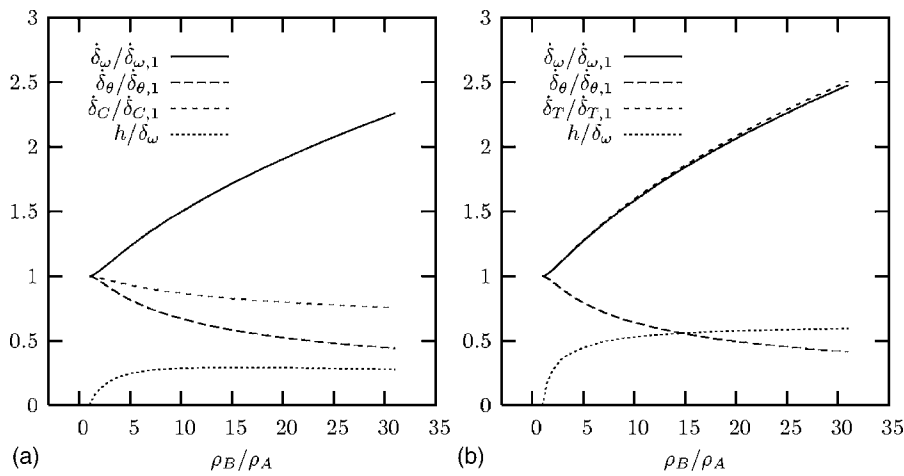


FIG. 7. Evolutions of the spreading rates and drift as functions of the density ratio. (a) Low-speed binary mixing. (b) Low-speed thermal mixing. The spreading rates are normalized by their constant-density value ($\rho_B/\rho_A = 1$), and the drift by the vorticity thickness.

remains centered so that h reduces to (minus) the z coordinate of the velocity-profile inflection point. When scaled by the value of the vorticity thickness (at the same density ratio), the drift can be seen to increase with the density ratio. Most of the increase is achieved before $\rho_B/\rho_A \approx 15$; for higher values of the density ratio, the scaled drift remains nearly constant (in fact, very slowly decreasing). In the situation of low-speed thermal mixing, the inflection point of the density profile is slightly above the axis [see Fig. 2(b)] and marginally contributes to the value of h . When scaled by the vorticity thickness, the drift is more than twice that observed for binary mixing, and it steadily increases with the density ratio.

The spreading rates obtained in the case of high-speed thermal mixing are plotted as functions of the Mach number in Fig. 8. The density ratio is set to unity and the spreading rates are normalized with their zero-Mach-number value. Here also, we notice the difference in the behavior of the

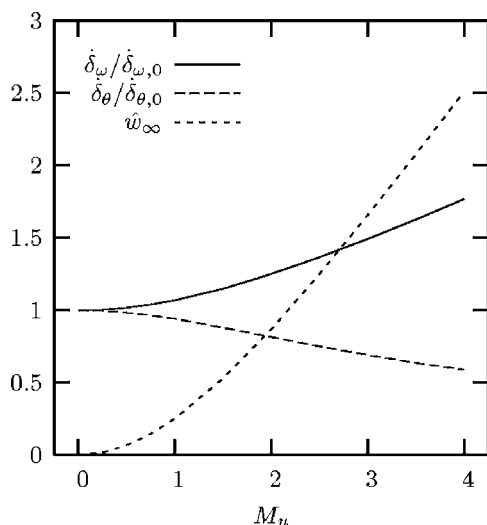


FIG. 8. Evolutions of the spreading rates and global deflection as functions of the Mach number. The spreading rates are normalized by their value at $M_u=0$. The deflection is quantified by the absolute value of the transverse velocity at infinity, normalized by the time-dependent velocity scale W_0 .

integral (momentum) and conventional (vorticity) thicknesses: The former decreases with the Mach-number value, whereas the latter increases.

Specific to the high-speed case is the presence of global deflection, a measure of which can be the absolute value of the similarity variable \hat{w} at infinity. This quantity is also plotted in Fig. 8; it can be seen to increase significantly with the Mach-number value. An appropriate rescaling of the plot would show that such an increase follows closely that of the vorticity thickness, so that the evolution of the spreading rate in this situation can obviously be attributed to advective growth.

V. CONCLUSION

Studying the case of the laminar time-evolving mixing layer provides basic information on the way variable density influences simple shear flows. Specific to the variable-density configuration is the generation of a transverse velocity field. Equation (7) for the divergence of the velocity field shows that such a deflection of the flow may result from either diffusive effects [mass or temperature mixing, term (c) or (d) of Eq. (7)], or dissipative effects [kinetic heating, term (b) of Eq. (7)].

In the first case, the homogenization of density due to the diffusive effects in the core of the mixing layer induces a macroscopic mass transfer from the heavy side of the flow toward its light side. Deflection of the flow results in some remarkable consequences: First, it directly produces a shift between the density and streamwise-velocity profiles: it could be said that the “shear layer” progressively drifts away from the “mixing layer.” Second, the transverse motion superimposed onto the main flow causes initially heavy fluid particles to be entrained backwards into the light stream. Finally, transport by the transverse velocity component is responsible for the thickening of the layer with increasing density ratio. In the case of binary mixing, where the value of the mass diffusivity per unit mass is a constant, the last effect is countered by the lessening of the diffusion coefficient at the light edge of the layer. It is important to note that, in such a situation, growth rates based on different variables

can exhibit opposite behaviors when the density ratio increases: the “mixing-layer” thickness can decrease while the “shear-layer” thickness increases.

When dissipation effects at high convective Mach number are considered, the dilatation effects due to heat release in the sheared region produce a global deflection with transverse velocities pointing from the core of the layer toward the heavy and light free streams, respectively. When the mixing layer between counterflowing streams is considered, this global deflection produces a tilting of the layer. However, in a coflowing mixing layer, it would produce a global drift of the mixing/shear layer toward the light side. In both cases, the thickening of the shear layer with increasing Mach numbers strictly corresponds to transport by the transverse velocity component (of dilatational origin) from the core of the flow.

To sum up, and with reference to the constant-density case, the variations in the growth rates observed in variable-density mixing layers originate from advective contributions superimposed onto the classical diffusive-growth mechanisms (observed in constant- and variable-density mixing layers, and directly linked to the diffusion terms present in the transport equations). Hence, we refer to this phenomenon as advective growth, specific to the variable-density situation.

Clarification of these issues should be useful in the analysis of more complex configurations. The space-evolving mixing layer is one instance of such flows; in this case, the transverse motion is usually associated with entrainment, but variable density obviously adds the specific contributions considered here. Investigating the mutual influences of entrainment and advective growth is likely to help the understanding of the physics involved in this flow. The case of the turbulent mixing layer is another instance in which the present analysis should be useful. Indeed, self-similarity cannot be assumed in this case (see, for instance, the discussion by de Bruyn Kops and Riley¹⁴), but turbulent diffusion and dissipation play qualitatively the same role as molecular diffusion and dissipation in the generation of the transverse motion. The simulation data of Pantano and Sarkar⁶ as well as their self-similar analysis of the turbulent mixing layer did exhibit drift and deflection. From the modeling point of view, the effect on the growth rates of the density dependence of the diffusion coefficients is probably a crucial issue. Catris and Aupoix¹⁵ mentioned that point when

dealing with the diffusion coefficients in the closure-quantities transport equations.

ACKNOWLEDGMENTS

The authors are indebted to an anonymous referee for pointing out the equivalence between tilting and global drift in the case of high-speed mixing; numerous suggestions for improvement of the paper are also acknowledged.

This work has been supported by the French Ministry of Education and Research and Ministry of Defense through Grant No. 03T590 and Contract No. DGA-DSP/ENSICA 03, respectively.

- ¹G. L. Brown and A. Roshko, “On density effects and large structures in turbulent mixing layers,” *J. Fluid Mech.* **64**, 775 (1974).
- ²D. Bogdanoff, “Compressibility effects in turbulent shear layers,” *AIAA J.* **21**, 926 (1983).
- ³G. L. Brown, “The entrainment and large structure in turbulent mixing layers,” in *Proceedings of the Fifth Australasian Conference on Hydraulics and Fluid Mechanics* (University of Canterbury, Christchurch, New Zealand, 1974), Vol. 1, pp. 352–359.
- ⁴P. E. Dimotakis, “Two-dimensional shear layer entrainment,” *AIAA J.* **24**, 1791 (1986).
- ⁵A. W. Vreman, N. D. Sandham, and K. H. Luo, “Compressible mixing layer growth rate and turbulence characteristics,” *J. Fluid Mech.* **320**, 235 (1996).
- ⁶C. Pantano and S. Sarkar, “A study of compressibility effects in the high-speed turbulent shear layer using direct simulation,” *J. Fluid Mech.* **451**, 329 (2002).
- ⁷A. Sanchez, M. Vera, and A. Linan, “Exact solutions for transient mixing of two gases of different densities,” *Phys. Fluids* **18**, 078102 (2006).
- ⁸F. Kozusco, C. E. Grosch, T. L. Jackson, C. A. Kennedy, and T. B. Gatski, “The structure of variable property compressible mixing layers in binary gas mixtures,” *Phys. Fluids* **8**, 1945 (1996).
- ⁹N. Lardjane, I. Fedioun, and I. Gökalp, “Accurate initial conditions for the direct numerical simulation of temporal compressible binary shear layers with high density ratio,” *Comput. Fluids* **33**, 549 (2004).
- ¹⁰P. Chassaing, R. A. Antonia, F. Anselmet, L. Joly, and S. Sarkar, *Variable Density Fluid Turbulence* (Kluwer Academic, Dordrecht, 2002).
- ¹¹P. Chassaing, “Some problems on single-point turbulence modeling of low-speed variable-density fluid motion,” in *IUTAM Symposium on Variable Density Low-Speed Turbulent Flows*, edited by L. Fulachier, J. L. Lumley, and F. Anselmet (Kluwer Academic, Dordrecht, 1997), pp. 65–84.
- ¹²S. K. Lele, “Flows with density variations and compressibility: Similarities and differences,” in *IUTAM Symposium on Variable Density Low-Speed Turbulent Flows*, edited by L. Fulachier, J. L. Lumley, and F. Anselmet (Kluwer Academic, Dordrecht, 1997), pp. 279–301.
- ¹³R. B. Bird, W. E. Stewart, and E. N. Lightfoot, *Transport Phenomena* (Wiley International, New York, 1960).
- ¹⁴S. M. de Bruyn Kops and J. J. Riley, “Re-examining the thermal mixing layer with numerical simulations,” *Phys. Fluids* **12**, 185 (2000).
- ¹⁵S. Catris and B. Aupoix, “Density corrections for turbulence models,” *Aerosp. Sci. Technol.* **4**, 1 (2000).